Available online at www.sciencedirect.com
SCIENCE DIRECT
Journal of Catalysis 241 (2006) 435–445
JOURNAL OF CATALYSIS
www.elsevier.com/locate/jcat

Hydrotreating of light cycled oil using WNi/Al_2O_3 catalysts containing zeolite beta and/or chemically treated zeolite Y

Lianhui Ding [a], Ying Zheng [a,*], Zisheng Zhang [b], Zbigniew Ring [c], Jinwen Chen [c]

[a] *Department of Chemical Engineering, University of New Brunswick, 15 Dineen Drive, PO Box 4400, Fredericton, NB, Canada E3B 5A3*
[b] *Department of Chemical Engineering, University of Ottawa, Canada, K1N 6N5*
[c] *National Centre for Upgrading Technology, 1 Oil Patch Drive, Suite A202, DEVON AB, Canada, T9G 1A8*

Received 2 March 2006; revised 3 May 2006; accepted 8 May 2006

Available online 21 June 2006

Abstract

Four W–Ni catalysts, containing Al_2O_3, chemically treated zeolite Y, hydrothermally treated zeolite beta, and the combination of the above zeolite Y and beta, were prepared. The catalysts were characterized by BET, NH_3-TPD, XRD, TEM, pyridine-IR, and XPS. The reaction performance in hydrodesulfurization (HDS), hydrodenitrogenation (HDN), and hydrodearomatation (HDA) was evaluated with light cycle oil (LCO). The zeolite-containing catalysts exhibited much higher HDN, HDS, and HDA activities than the WNi/Al_2O_3. The three zeolite-containing catalysts had similar HDN activity. The WNi/Beta + Y and WNi/Beta catalysts had higher HDS activity than the WNi/Y catalyst. The higher HDN, HDS, and HDA activities of the three zeolite-containing catalysts are associated primarily with enhanced hydrogenation activity and increased acidity.

Keywords: Catalysts; Zeolite Y; Zeolite beta; Hydrotreating; LCO

1. Introduction

Imminent legislation demands that the sulfur content in diesel fuel be reduced to <15 ppm [1]. Such low sulfur content cannot be readily achieved using conventional hydrogenation catalysts and processes. Most of the remaining sulfur species after the conventional hydroprocessing treatment are composed of 4,6-substituted dibenzothiophenes (DBTs) [2]. The steric hindrance of substituting groups in the 4,6-position of DBT molecules makes conversion by hydrogenation or hydrogenolysis almost impossible [3–5]; however, hydrodesulfurization (HDS) activity of 4,6-substituted DBT can be greatly improved by the hydroisomerization, which shifts one substituting group from the 4 or 6 position to the 3 or 7 position, where the steric hindrance can be relieved and HDS reactions can more readily occur [6,7].

The hydroisomerization activity of a catalyst can be imparted by the addition of acidic component zeolites in catalysts [8]. Among the zeolites available, zeolite Y is the most widely applied and most extensively studied due to its appropriate pore structure, high acidity, and good thermal and hydrothermal stability [9–13]. Although acidic zeolite helps enhance HDS activity of the catalysts, the incorporation of acidic zeolites will also increase the deactivation and overcracking of diesel fractions, which lowers the yield of the diesel fuel and increases hydrogen consumption. To improve the HDS activity of refractory sulfur species and avoid the rapid deactivation and overcracking of the diesel distillates, the surface acidity of zeolite should be properly modified. Studies show that zeolite Y without any treatment is less active in hydrotreating than the conventional NiMo/Al_2O_3 catalyst alone, and that the incorporation of Ni-exchanged Y zeolite in NiMo/Al_2O_3 improves the activity only slightly [14].

As-synthesized zeolite HY has a high acid concentration but a low acid strength. The strength of acid sites plays a more important role than the surface density in HDS reactions [15,16]. One effective way to increase acidic strength is to remove some

* Corresponding author. Fax: +1 506 453 3591.
E-mail addresses: lianhui.ding@unb.ca (L. Ding), yzheng@unb.ca (Y. Zheng), jzhang@genie.uottawa.ca (Z. Zhang), zring@NRCan.gc.ca (Z. Ring), jichen@NRCan.gc.ca (J. Chen).

0021-9517/$ – see front matter
doi:10.1016/j.jcat.2006.05.004

tetrahedron Al atoms $[AlO_4]^-$ from the framework of zeolites. The removal of framework aluminum can be achieved by hydrothermal or chemical treatment [17]. The extra-framework aluminum (EFAL) stays in the hydrothermally treated zeolite and can produce a selectivity pattern different from that expected from the framework aluminum content [18]. By chemical treatment with $(NH_4)_2SiF_6$ in aqueous solution, aluminum is extracted from the framework, while silicon is inserted back in the vacancies left by the aluminum. The dealuminated Y prepared by this approach does not contain any EFAL and has very little Lewis acidity [19]. Therefore, it is assumed that the zeolite treated by the $(NH_4)_2SiF_6$ solution will exhibit different performance in HDS and hydrodearomatation (HDA) of diesel fractions.

Another large-pore zeolite similar to zeolite Y, zeolite beta, has a high SiO_2/Al_2O_3 ratio and exhibits higher hydroisomerization activity, lower hydrogen-transfer capacity, and lower catalyst deactivation by self-poisoning [20–22]. These features make zeolite beta a good catalyst component for converting refractory sulfur species and decreasing catalyst deactivation.

Previous studies have focused mainly on the application and comparison of the two zeolites in the hydrocracking of heavy oil [13,15,16,22]. Little research has been done on HDS, especially the hydrotreating performance of real inferior diesel fractions using chemically treated zeolite Y and zeolite beta as acidic components of the catalyst. The main objective of this study is to investigate the hydrotreating performance of the W–Ni catalysts prepared by chemically treated zeolite Y and zeolite beta using light cycle oil (LCO) as a feedstock.

2. Experimental

2.1. Preparation of zeolites

All of the chemicals used in preparing the zeolites and the catalysts were purchased from Sigma–Aldrich. NH_4-beta (Zeolyst CP814E) was calcinated at 813 K for 10 h, then treated with 0.5 M hydrochloric acid aqueous solution at 353 K for 2 h under stirring. After separation, the filtrated cake was treated in an autoclave reactor at 873 K and 0.2 MPa for 2 h.

Chemically modified zeolite Y was synthesized as described previously [23]. In a flask, 95 g of NH_4NaY (Zeolyst CBV-300) was stirred with a 1.0 M ammonium acetate solution at 348 K, after which 200 mL of 0.8 M $(NH_4)_2SiF_6$ solution was added in a dropwise manner to the flask. The sample was stirred at 368 K for 24 h, thoroughly washed with boiling water, and then dried at 383 K overnight. The dried sample was hydrothermally treated at 823 K and 0.1 MPa for 1 h in an autoclave reactor.

The main properties of the starting material and final zeolite products are summarized in Table 1.

2.2. Catalyst preparation

The supports were prepared by mixing the zeolites, large-pore alumina (Sasol PURALOX TH100/150, pore volume: 0.96 mL/g, surface area: 201.6 m^2/g), and a binder (partially acid-peptized alumina, SASOL, CAPAPAL B), extruded to form cylindrical extrudates, dried at 383 K overnight, and then calcined in air at 823 K for 4 h. The NiW catalysts were prepared by coimpregnation of the above extrudates using the incipient wetness method with an aqueous solution of the appropriate amount of nickel nitrate hexahydrate $[Ni(NO_3)_2{\cdot}6H_2O]$ and ammonium metatungstate $[(NH_4)_6H_2W_{12}O_{40}]$, dried at 383 K overnight, and then calcinated at 773 K for 4 h. The catalysts prepared from the supports containing Al_2O_3, 15 wt% modified zeolite Y, 15 wt% modified zeolite beta, and 15 wt% modified zeolite beta plus 15 wt% zeolite Y were designated as WNi/Al_2O_3, WNi/Y, WNi/Beta, and WNi/Beta + Y, respectively. All catalysts had a nominal WO_3 content of 24 wt% and a nominal NiO content of 6 wt%.

Table 1
Properties of starting material and final zeolite products

	Beta	Y
Before modification		
SiO_2/Al_2O_3 molar ratio	25.0	5.1
Na_2O	0.05	2.8
Surface area (m^2/g)	710	925
Pore volume (mL/g)	0.40	0.42
Unit cell size (Å)		24.68
Acidity[a] (mmol/g)	0.935	–
After modification		
Na_2O	0.04	0.08
Surface area (m^2/g)	636	704
Pore volume (mL/g)	0.36	0.32
Relative crystallinity[b] (%)	85	102
Unit cell size (Å)		24.33
Acidity[a] (mmol/g)	0.201	0.482

[a] Obtained from pyridine infrared spectroscopy.
[b] Relative to starting zeolite.

2.3. Catalyst characterization

2.3.1. NH_3 temperature-programmed desorption (NH_3-TPD)

First, 0.5 g of a 30- to 40-mesh sample was loaded into a 5-mL tubular reactor, then purged for 2 h with 40 mL/min of helium at 773 K (increased from ambient temperature to 773 K at 5 K/min), followed by a temperature decrease to 353 K. Next, 50 mL/min of gaseous ammonia mixed with 40 mL/min of helium was charged for 30 min at 353 K, then purged with 40 mL/min of He at 373 K for 1 h. Under the 40 mL/min of helium, the temperature was raised from 373 to 883 K at a rate of 15 K/min, and the desorbed ammonia was analyzed by mass spectroscopy.

2.3.2. Powder X-ray diffraction (XRD)

The crystallinity and phase purity of solid products were characterized using a Bruker AXS D8 ADVANCE, with Cu-K_α radiation provided by a graphite monochromator.

2.3.3. Transmission electron microscopy (TEM)

TEM was performed on a JEOL 2010 STEM, operated at 200 keV. The spectra were collected using an EDAX Genesis 4000 system. Samples were prepared by the drop method. A small amount of sulfided catalyst powder was sonicated in

100% ethanol. One drop was removed with a micropipette and dropped onto a copper (or nickel) support grid. The sample was then lightly coated with carbon to reduce charging in the TEM.

2.3.4. X-ray photoelectron spectroscopy (XPS)

XPS spectra of the samples were obtained using a VG Microtech MultiLab ESCA 2000 system with a CLAM4 hemispherical analyzer. The hemispherical analyzer consists of an analysis chamber for taking the XPS spectra, which was operated under a vacuum $<4 \times 10^{-10}$ mbar, and a fast entry air lock for sample introduction. The source was nonmonochromatized Mg-K_α X-rays at 1253.6 eV (15 kV, 20 mA). To sample a deeper depth, photoelectron detection perpendicular to the sample surface was chosen. The high-resolution C 1s spectrum of the adventitious hydrocarbon (at 284.5 eV) on the sample surfaces were recorded before and after each measurement and used as a reference for charge correction. Quantitative information of surface composition was obtained from integrated peak intensities and atomic sensitivity factors using the Advantage data acquisition and processing software (Thermo VG Scientific). Peak fits of all spectra were performed using the Shirley background correction and Gaussian–Lorentzian curve synthesis.

2.3.5. BET

Nitrogen adsorption measurements were performed on a Quantachrome Autosorb-1. Before adsorption, the samples were calcined at 823 K for 16 h. Powder samples of 30–40 mg were degassed in a sample preparation station under 473 K and a vacuum of 1.33×10^{-3} Pa for 15 h, then switched to the analysis station for adsorption and desorption at 77 K in liquid nitrogen. Surface area was calculated with the multipoint BET equation with linear region in the P/P_0 range of 0.05–0.35. Pore volume was calculated from the maximum adsorption amount of nitrogen at $P/P_0 = 0.99$.

2.3.6. Pyridine infrared (IR)

Adsorbed pyridine IR spectra were recorded on a BIO-RAD FTS-60 Spectrometer. Samples of 10 mg were grounded, pressed to form 1-cm-diameter wafers, and installed on supports. The sample cell was heated to 573 K under vacuum (1.33×10^{-3} Pa) overnight and then cooled to room temperature. Pyridine was then introduced into the cell, and the adsorption was performed. The excess and physically adsorbed pyridine was evacuated under vacuum at room temperature overnight. IR spectra in the range of 1000–4000 cm^{-1} were recorded.

2.4. Catalyst activity evaluation

The evaluation of catalyst activity was carried out in a 1-L stirred autoclave (Autoclave Engineers Eze-Seal stirred reactor) with LCO. The properties of LCO are given in Table 2. In the evaluation, 20 g of catalyst were loaded into the catalyst basket in the reactor, and the reactor was repeatedly vacuumed and refilled with hydrogen to replace the air in the autoclave.

Table 2
Properties of LCO feed

Density (g/mL) (298 K)	0.9591
Nitrogen (ppm)	495.6
Sulfur (wt%)	1.3
Saturates (wt%)	12.4
Monoaromatics (wt%)	19.0
Diaromatics (wt%)	47.0
Polyaromatics (wt%)	21.6
Distillation (K)	
0.5 wt%/10 wt%	406/487
20 wt%/30 wt%	508/527
40 wt%/50 wt%	540/555
60 wt%/70 wt%	574/591
80 wt%/90 wt%	611/635
95 wt%	650

Then 5 mL of sulfiding agent, dimethyl disulfide (DMDS), were sucked into the reactor. (Theoretical calculation and experimental results on DMDS decomposition have demonstrated that 5 mL of DMDS is sufficient to sulfide 20 g of catalyst.) Before heating, the reactor was pressurized to 3.4 MPa. The catalyst was sulfided in situ at 593 K for 2 h and at 633 K for another 2 h. After the sulfidation, 200 g of LCO was charged into the batch autoclave reactor through a feed-charging tank mounted on the top of the reactor. The reactor was pressurized to 4.8 MPa, and the temperature was increased to 648 K at a rate of 3 K/min under the 1000-rpm stirring. When the temperature reached the set value, the hydrogen pressure was adjusted to 8.8 MPa. When the pressure drop rate was <10 kPa/min, the pressure was once again raised to 8.8 MPa. The evaluation was completed when the pressure became nearly constant. The liquid product was collected and analyzed. The nitrogen, sulfur, and aromatics were analyzed according to ASTM D4629, ASTM D4294, and ASTM D6591, respectively. The boiling ranges of LCO and liquid products were measured with simulated distillation (SimDis) by gas chromatography. The conversion was based on the initial boiling point of the feed (406 K) and liquid yield. The conversion was calculated from the following equation:

$$x = x_1 + 100\% \times (200 - x_2)/200,$$

where x is conversion, x_1 is the weight percentage of the fractions below 406 K in the all-liquid product, and x_2 is the weight (in g) of liquid product collected from reactor. The HDS, hydrodenitrogenation (HDN), and HDA activities are defined as the percent removal (conversion) of sulfur, nitrogen, and aromatics, respectively.

3. Results and discussion

3.1. Textural and acidity properties

Textural properties of the four catalysts are listed in Table 3. As expected, the surface areas of WNi/Y and WNi/Beta + Y increased and the pore volumes decreased when zeolites were introduced to the catalyst support. However, the addition of 15 wt% of zeolite beta did not increase the surface

Table 3
Textual and acidity properties of the catalysts

	WNi/Al_2O_3	WNi/Beta+Y	WNi/Y	WNi/Beta
Pore volume (mL/g)	0.56	0.38	0.37	0.42
Surface area (m^2/g)	165	222	221	165
Average pore size (nm)	13.6	6.8	6.7	10.2
Total acidity (mmol/g_{cat})	0.340	0.546	0.506	0.480
Acidity distribution (mmol/g)				
Weak	0.181 (53.2)[a]	0.246 (45.1)	0.302 (59.7)	0.216 (45.1)
Medium	0.08 (23.6)	0.130 (23.8)	0.124 (24.5)	0.113 (23.5)
Strong	0.08 (23.2)	0.170 (31.1)	0.08 (15.8)	0.151 (31.5)
Average length of slabs[b] (nm)	8.7	26.3	17.7	16.1
Average number of layers[b]	2.0	3.7	4.4	3.7

[a] The value in the parentheses is the percentage of various strength of acid.
[b] Obtained from TEM.

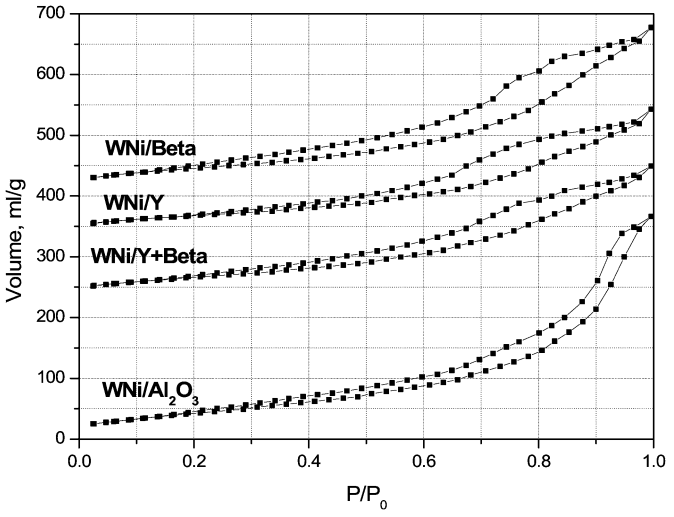

Fig. 1. Isotherms of WNi/Al_2O_3, WNi/Beta, WNi/Y, and WNi/Beta + Y.

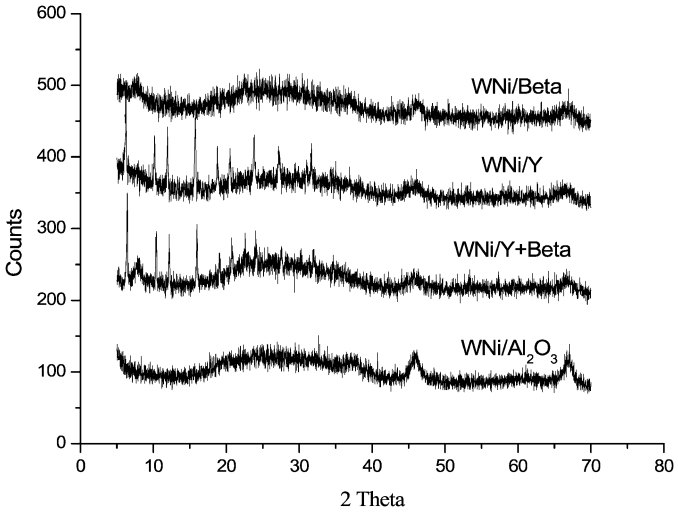

Fig. 2. XRD profiles of WNi/Al_2O_3, WNi/Beta, WNi/Y, and WNi/Beta + Y.

area of WNi/Beta compared with that of the reference catalyst WNi/Al_2O_3. This can also be seen from the isotherm profiles in Fig. 1. In comparison with WNi/Y, the extent of decrease in the pore volume and average pore size of WNi/Beta was much lower, even though similar isotherm profiles of the three zeolite-containing catalysts were obtained (Fig. 1). The larger pore size makes WNi/Beta more favourable for the diffusion of reactants and products compared with WNi/Beta + Y and WNi/Y.

The acidities and their distribution of the four catalysts are listed in Table 3. To compare the acidity distribution among the catalysts, the weak, medium, and strong acidities were assigned to the peak areas of NH_3-TPD curves below 623 K, at 623–773 K, and above 773 K, respectively. Comparing the acidity of WNi/Al_2O_3, the addition of zeolite beta and Y enhanced the overall acidity. The increase in acidity for zeolite Y was higher than that for the zeolite beta. The incorporation of the zeolite Y led mainly to an increase in weak acidity, whereas incorporation of the zeolite beta caused an increase in strong acidity. Compared with WNi/Beta and WNi/Y, even though the zeolite content doubled, the total acidity and the proportion of the strong acidity of WNi/Beta + Y increased only slightly, suggesting that almost half of the acidic sites were occupied by hydrogenated metals or aluminum species. Apparently, the modified zeolite Y caused mainly an increase in total acidity, and the zeolite beta enhanced the strong acidity.

3.2. XRD

The XRD profiles of the oxidic samples are shown in Fig. 2. No detectable XRD crystallines of WO_3, NiO, $Al(WO_4)_3$, or $NiAl_2O_4$ were present in the oxide catalysts. This means that the tungsten and nickel oxidic species were either completely amorphous or composed of crystallites smaller than 4 nm. The WO_3 and NiO were considered evenly distributed on the surface of the support. The characteristic diffraction peaks of γ-Al_2O_3 appeared in all samples. The characteristic diffraction peaks for zeolite Y (2θ 12°, 16°, 19°, 20°, and 24°) were detected for two of the zeolite Y-containing catalysts, and the characteristic diffraction peaks for zeolite beta (2θ 22.4° and 6°) were detected for two of the zeolite beta-containing catalysts. The crystallinity of all zeolites was greatly reduced, especially that of WNi/Beta. WO_3 loading is known to decrease the crystallinity of zeolite [24] and may be the cause of the reduced crystallinity observed here.

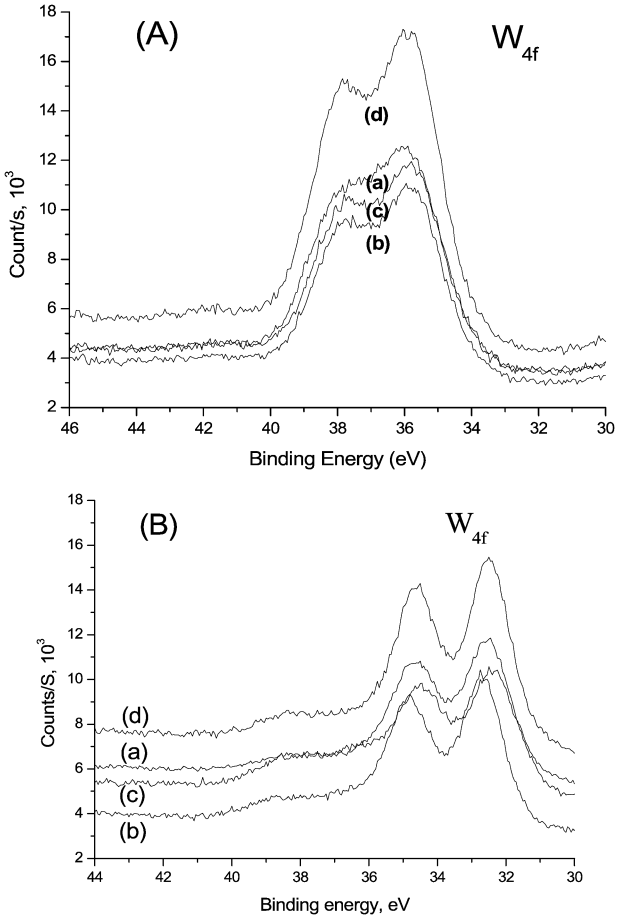

Fig. 3. XPS W 4f spectra of oxidic (A) and sulfided (B) W–Ni catalysts: (a) WNi/Al_2O_3, (b) WNi/Beta + Y, (c) WNi/Beta, and (d) WNi/Y.

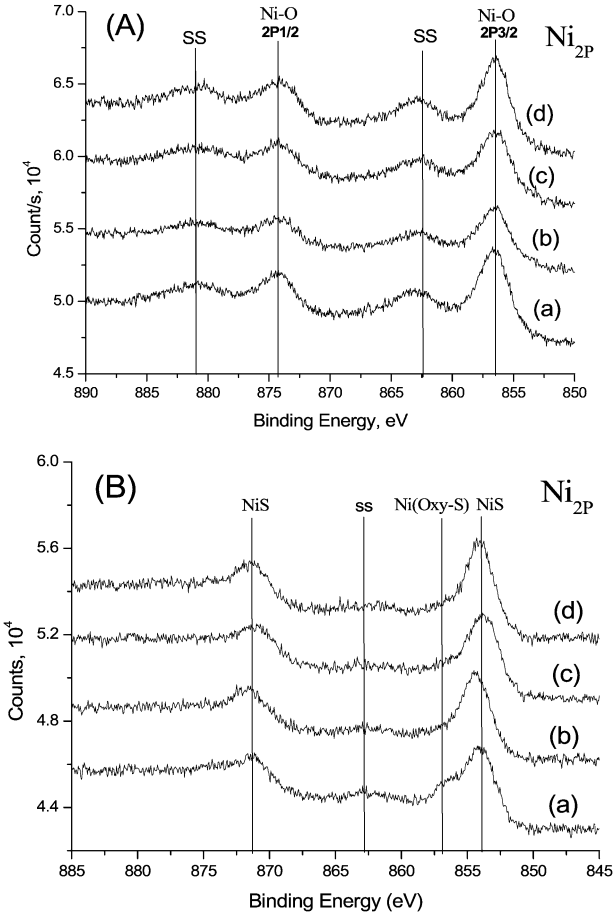

Fig. 4. XPS Ni 2p spectra of oxidic (A) and sulfided (B) WNi catalysts: (a) WNi/Al_2O_3, (b) WNi/Beta + Y, (c) WNi/Beta, and (d) WNi/Y.

3.3. XPS

3.3.1. Surface species of oxidic and sulfided catalysts

Figs. 3 and 4 show XPS spectra of the four oxidic and sulfided W–Ni catalysts. Table 4 summarizes the binding energies (BEs) of W, Ni, and S for oxidic and sulfided samples. The spectra of the oxidic catalysts show a doublet peak of W $4f_{5/2}$ and W $4f_{7/2}$ electrons at BE positions of 37.8–37.9 and 35.7–35.8 eV, respectively. These peaks are assigned to W^{6+} species, most likely $W^{6+}O_3$ [25,26]. WNi/Al_2O_3 exhibits higher BEs of W 4f and Ni 2p core levels compared with those for zeolite-containing samples, suggesting that adding the zeolites weakened the interaction of tungsten with the support and/or the Ni atoms. The effect of high-silica/alumina ratio zeolite beta on the electronic state of tungsten atoms was more pronounced than that of zeolite Y. The two main peaks in the Ni 2p X-ray photoelectron spectra of the oxidic samples were assigned to the spin-splitting Ni $2p_{3/2}$ (BE 856.4 eV) and Ni $2p_{1/2}$ (BE 873.8 eV), and the two broad peaks were assigned to the envelopes of the corresponding shakeup satellite (SS) lines [11].

After sulfidation, a second doublet peak appeared at 34.4 and 32.5 eV (Figs. 3B and 4B), which is typical for tungsten with a formal charge state of +4 as in the WS_2 phase [12]. The Ni $2p_3$ XPS spectra of the sulfided catalysts present a relatively intense peak at about 854 eV, and a second broad band overlapped partially with the first one, with a BE of about 856 eV. The intense peak of Ni $2p_1$ appeared at about 871 eV. The shape of the Ni 2p envelope with a satellite peak at 862 eV clearly showed the presence of nonsulfided Ni^{2+} species in all catalysts after sulfidation. The Ni $2p_3$ peak at 856 eV was also due to the pres-

Table 4
Binding energies of core levels of the components for oxidic and sulfided forms of W–Ni catalysts

Sample	WNi/Al_2O_3	WNi/Beta + Y	WNi/Y	WNi/Beta
Oxidic				
W $4f_7$	35.81	35.67	35.72	35.68
W $4f_5$	37.89	37.80	37.86	37.82
Ni $2p_3$	856.67	856.33	856.36	856.45
Ni $2p_1$	874.27	874.08	874.00	874.34
Ni $2p_3$ SS	862.66	862.86	862.79	862.69
Ni $2p_1$ SS	880.75	880.83	880.58	880.98
Sulfided				
W $4f_7$	32.51	32.66	32.48	32.27
W $4f_5$	34.70	34.83	34.66	34.45
Ni $2p_3$	853.79	854.17	853.90	853.47
Ni $2p_1$	871.04	871.42	871.15	870.66
Ni $2p_3$ oxy-S	856.25	855.89	855.89	855.68
Ni $2p_3$ SS[a]	862.44	862.71	862.41	862.37
Ni $2p_1$ SS[a]	878.26	876.42	877.46	877.80
S 2p	162.04	162.2	161.98	161.81

[a] SS: shakeup satellites.

ence of the nonsulfided Ni^{2+} species [27–29]. The second Ni $2p_{3/2}$ peak at 853.1–853.7 eV, together with the presence of the S $2p_{3/2}$ peak at 162 eV, was associated with nickel sulfides [28,30].

The S 2p spectra of all the sulfided catalysts exhibited one peak at the BE value of 162.0 ± 0.2, which can be assigned to S^{2-} [24,30]. No other signal was identified around a BE of 169 eV, indicating that no sulfate species existed, and thus no oxidation of the catalysts occurred during the transfer of the solid from the sulfiding reactor to the XPS chamber [31].

3.3.2. The sulfiding degree of W and Ni

Studies revealed that only W(Mo) and Ni(Co) in the hydrogenation catalyst can be sulfided; no sulfidation occurred to the supports [32]. Therefore, the sulfidation degree of the hydrogenation catalyst can be estimated by the atomic ratios of S/W + Ni. If the W–Ni catalyst with a W/Ni atomic ratio of 1.29 is fully sulfided, and the fully sulfided W and Ni species are taken as WS_2 and Ni_3S_2 [33–35], then the S/(W + Ni) atomic ratio should be 1.42. Due to the incomplete sulfidation of W and Ni species and the same BE of different sulfur ligands in XPS [32], no significant values could be calculated from the S/W + Ni ratio, which makes an accurate relative qualification impossible. Only a rough evaluation of the overall sulfidation degree can be made using the S/W + Ni obtained from XPS intensity ratios. The values are summarized in Table 5.

In addition, preliminary evaluation of the Ni $2p_{3/2}$ emission line of the sulfided catalysts indicated that two contributions, an oxidic one and a sulfidic one, could be identified. Therefore, the sulfidation extent of Ni can be determined by the relative integrated area ratio of the peaks corresponding to the sulfided Ni and oxided Ni. However, the results do not allow a direct quantitative interpretation in terms of the various Ni species [36]. The data in Table 5 reflect changes only in the relative peak areas in the main Ni $2p_{3/2}$ emission line and should be considered only a semiquantitative trend for the transformation in the Ni speciation on sulfiding. The extent of sulfidation of W species was calculated based on the atomic concentration ratios of the corresponding sulfide species over the total oxide and sulfide species. These data are also reported in Table 5.

Table 5
XPS intensity ratios for oxidic and sulfided forms of W–Ni catalysts

Sample	WNi/Al_2O_3	WNi/Beta + Y	WNi/Y	WNi/Beta
Bulk W/Ni molar ratio	1.29	1.29	1.29	1.29
Bulk W/Si + Al, ×100	15.1	11.8	13.3	13.2
Bulk Ni/Si + Al, ×100	11.7	9.2	10.3	10.2
Oxidic ×100				
I_W/I_{Al+Si}	6.35 (58)[a]	7.80 (34)	8.47 (36)	7.67 (41)
I_{Ni}/I_{Al+Si}	6.28 (15)	6.05 (34)	5.72 (44)	6.10 (40)
I_W/I_{Ni}	1.01	1.29	1.48	1.26
Sulfided ×100				
I_W/I_{Al+Si}	4.15 (35)[b]	5.78 (26)	6.52 (23)	5.50 (28)
I_{Ni}/I_{Al+Si}	3.55 (43)	4.72 (22)	4.39 (23)	4.40 (28)
I_W/I_{Ni}	1.17	1.22	1.49	1.25
S/W + Ni	1.58	1.49	1.53	1.47
Degree of sulfiding				
WS_2	91.3	87.8	92.0	84.4
NiS	77.1	93.5	90.4	87.3

[a] The values in the parentheses in the oxidic section are the percentage of the W or Ni reduction from bulk W or Ni/Si + Al ratio to oxidic state.
[b] The values in the parenthesis are the percentage of the W or Ni reduction from oxide state to sulfided state.

The S/W + Ni ratios for all catalysts are >1.42, suggesting that very small tungsten and/or nickel sulfide clusters contained more than the stoichiometric amount of sulfur [37]. The more than stoichiometric amount of sulfur can be attributed to the formation of element sulfur during sulfidation [33,38]. From the XPS spectra shown in Fig. 3B, it can be noted that the base line at ca. 38 eV was not zero. A broad band assigned to remaining oxidic species of W indicates that the W species were not completely sulfided. In all catalysts, W and Ni had a very high degree of sulfidation. The sulfided W species ranged from 84.4 to 92.0%, and the sulfided Ni species ranged from 77.1 to 93.5%. The sulfidation degree of Ni in WNi/Al_2O_3 was much lower than that of the other three zeolite-containing catalysts, demonstrating that more nickel species interacted strongly with the support and could not be sulfided. Among the zeolite-containing catalysts, the sulfidation degree decreased in the following order: WNi/Y > WNi/Beta + Y > WNi/Beta. No obvious relationship could be established between S/W + Ni and the sulfidation degree of both W and Ni, but the changing trend of S/W + Ni and W sulfidation degree was similar.

3.3.3. Surface atomic ratios

Compared with WNi/Al_2O_3, the zeolite-containing catalysts have different textural properties and contain specific amounts of surface Si species. The various pore systems and existence of Si species cause the variations in the distribution of Mo and Ni species. Ni ions can readily enter into zeolite channels and tend to be evenly distributed across the support, whereas Mo species are preferentially distributed on the surface of Al_2O_3 [10,39]. When calcinated and sulfided, the redistribution of Ni and Mo species also occurs in a different way on WNi/Al_2O_3 from on the zeolite-containing catalysts, due to their different porous systems and surface species. The surface atomic ratios by XPS can well reflect the differences in Mo and Ni distributions, especially the distribution changes with the calcination and the sulfidation. To obtain information on the dispersion of surface species, the surface atomic ratios of Ni/Si + Al and W/Si + Al derived from XPS for each catalyst are given in Table 5. The bulk W/Ni, W/Si + Al, and Ni/Si + Al atomic ratios were calculated based on the W, Ni, alumina, and crystalline aluminosilica zeolite added during the catalyst preparation. The W/Si + Al and Ni/Si + Al ratios of all oxidic catalysts were much lower than the bulk ratios (11.8–15.1 for W/Si + Al and 9.2–11.7 for Ni/Si + Al), suggesting that a considerable amount of W and Ni migrated into the bulk and most likely into the pores or cavities of support after calcination. More W and less Ni migrated into support for WNi/Al_2O_3 than for the other three zeolite-containing catalysts. More W and slightly less Ni were reduced on the surface for WNi/Beta than for WNi/Y. In WNi/Beta + Y and WNi/Beta, the reduction of W and Ni on the surface was nearly identical.

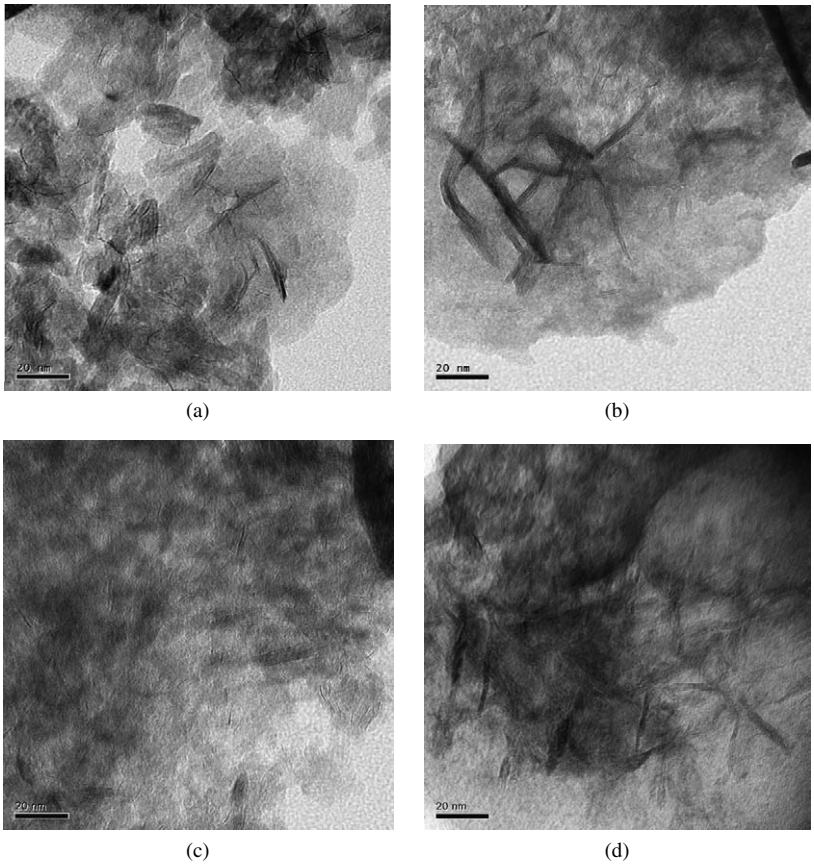

(a) (b) (c) (d)

Fig. 5. TEM images of (a) WNi/Al_2O_3, (b) WNi/Beta + Y, (c) WNi/Y, and (d) WNi/Beta (the scale bar in each picture is 20 nm).

After sulfidation, the amount of the surface W and Ni decreased further. The reduction of W and Ni for WNi/Al_2O_3 was still much greater than that for the other three zeolite-containing catalysts. The surface W and Ni decreased in almost the same proportion for the three zeolite-containing catalysts.

3.4. TEM

The representative TEM images of the four sulfided catalysts are shown in Fig. 5. The TEM images reveal the presence of typical structures of the layered WS_2 phase (confirmed by EDX). No large aggregates of WS_2 were observed. In the sulfided state, the WS_2 slabs were formed on the surface of all catalysts and exhibited thread-like layers. In analyzing WS_2 slabs, the following were assumed: (1) WS_2 slabs were oriented parallel to the support (basal up), (2) the thickness of the slabs was similar to and less than 4 nm, and (3) WS_2 slabs are randomly arranged on the support in term of the direction of the electron beam of XPS. The average number of layers per slab and average slab length were calculated from the measurement of about 300 crystallites with the following equations:

$$\text{average slab length} \quad \overline{L} = \left(\sum_{i=1}^{n} n_i l_i\right) \Big/ \sum_{i=1}^{n} n_i$$

and

$$\text{average number of layers} \quad \overline{N} = \left(\sum_{i=1}^{n} n_i N_i\right) \Big/ \sum_{i=1}^{n} n_i,$$

where l_i is the length of the slab particle, n_i the number of the particles with the l_i length or N_i layers, and N_i the number of layers in the particle i. The average slab length was determined by manually measuring the WS_2 slabs with the software along with the TEM on 7–9 TEM images taken at different areas of the sample. The statistical results of the average length and number of layers of the WS_2 slabs are given in Table 3. The slab length (Fig. 6a) and layer number (Fig. 6b) distributions are illustrated in Fig. 6. For the WNi/Al_2O_3 catalyst (Fig. 5a), the average particle length is equal to 8.7 nm and the average layer number is equal to 2.0, which are close to the values of 7.3 nm and 2.4 reported in the literature [40]. When the 15 wt% zeolites (beta or Y) were added into the catalyst (WNi/Beta and WNi/Y), the average length of the WS_2 slabs increased to 16.1–17.7 nm, and the average layer number increased to 3.7–4.4 (Fig. 5d and 5c). When the zeolite content increased further 30 wt% (WNi/Beta + Y), the average slab length also further increased to 26.3 nm, whereas the average layer number nearly unchanged (3.7) (Fig. 5b). Meanwhile, with increased zeolite content, along with the increasing average length of WS_2 slabs and average layer numbers, the morphology of the WS_2 structures on WNi/Y, especially on WNi/Beta + Y (Fig. 5b) became more curved and tended to be superimposed. The curved structure can result in a large static disorder of the W–W distances. Such curved sites in the WS_2 crystallites probably cause more vacant sulfur sites, and more catalytically active sites may be formed. As shown in Fig. 7, there existed a good linear rela-

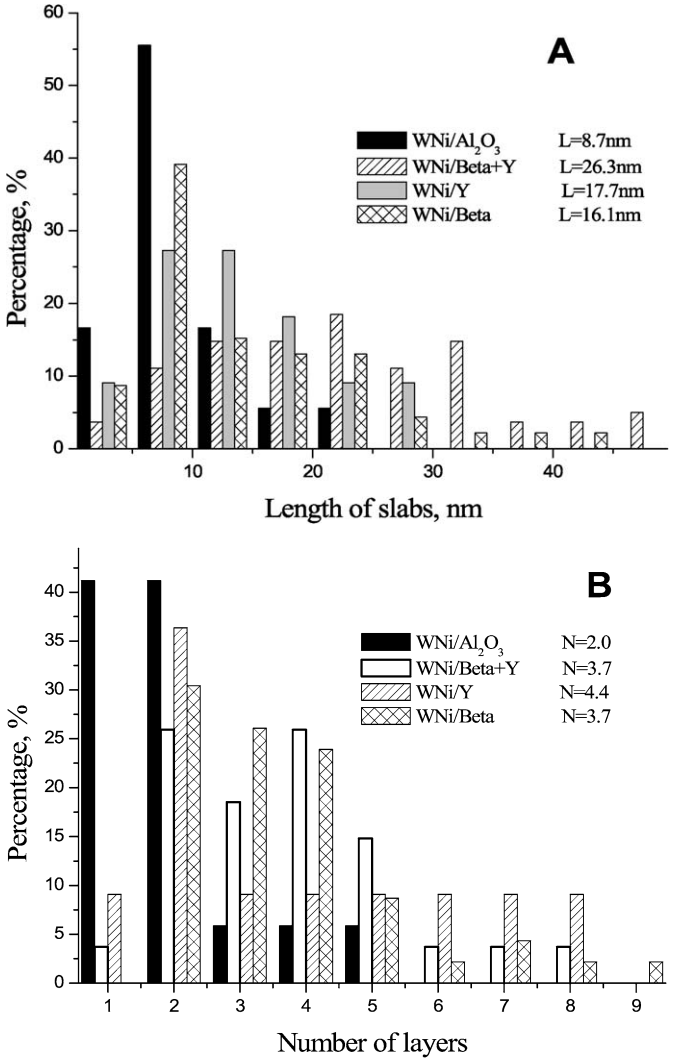

Fig. 6. Crystal size distribution of WS_2 for sulfided catalysts: slab length (A), number of layers (B).

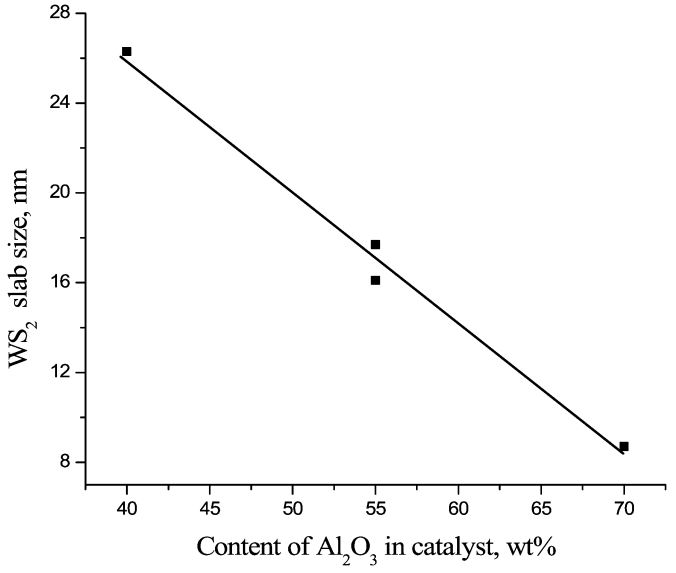

Fig. 7. The relationship between WS_2 slab size and the content of Al_2O_3 in catalyst.

Table 6
Evaluation in 1 L autoclave with LCO

Catalyst	WNi/Al_2O_3	WNi/Beta + Y	WNi/Y	WNi/Beta
Density (g/mL) (288 K)	0.9264	0.9009	0.9136	0.9171
Nitrogen (ppm)	97.88	1.42	1.84	6.14
Sulfur (ppm)	507	165	355	232
>685 K fraction (wt%)	0.9	2.1	2.5	1.5
Liquid yield (wt%)	92.3	90.3	88.5	91.5
Conversion from distillation curve	0.85%	3.70%	0.80%	1.55%
Conversion (wt%)	8.55	12.40	12.30	10.05
Cetane index[a]	26.8	27.7	26.9	27.4

[a] Calculated based on ASTM D976.

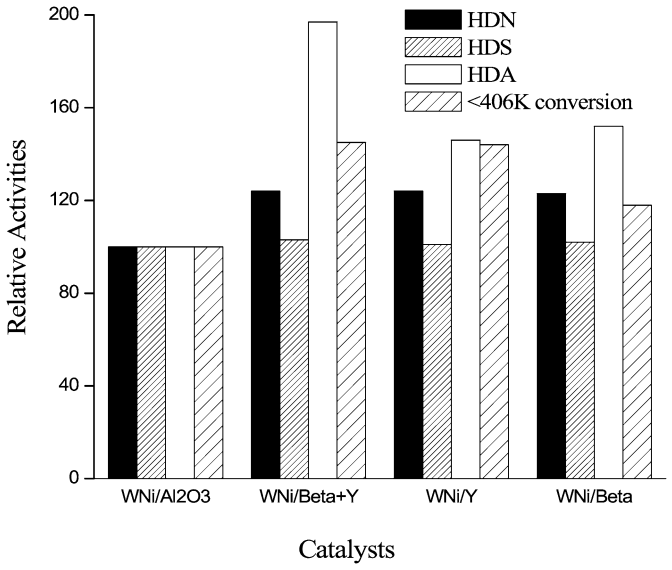

Fig. 8. Relative HDS, HDN, and HDA activities, and <406 K conversion on WNi/Al_2O_3, WNi/Beta, WNi/Y, and WNi/Beta + Y.

tionship between the average length of the WS_2 slab and the Al_2O_3 content in the catalysts, suggesting that the size of WS_2 is mostly related to the distribution of WS_2 on the surface of Al_2O_3, irrespective of the type of zeolites. This was also confirmed by EDX analysis, demonstrating that WS_2 was distributed mainly on the Al_2O_3 part of the zeolite-containing support. Compared with WNi/Al_2O_3, the distribution of the slab length and the layer number for the zeolite-containing catalysts were much broader (Fig. 6), probably due to the coexistence of Al_2O_3 and zeolite. On Al_2O_3, shorter slabs and fewer layers of WS_2 were formed. In contrast, longer slabs with more layers on the zeolite surface were distributed on the catalyst surface.

3.5. Activity evaluation

The LCO hydrotreating results are summarized in Table 6 and Figs. 8–10. The LCO used in this experiment, characterized by high density, high aromatic content, and high sulfur content, is a typical inferior feedstock for hydrotreatment. Compared with WNi/Al_2O_3, the zeolite containing catalysts exhibit much higher HDN, HDS, and HDA activities (Fig. 8). The HDS, HDN, and HDA activities increased by 1.17–2.63 wt%, 18.51–19.45 wt%, and 3.3–6.9 wt%, respectively. About 99 wt% of

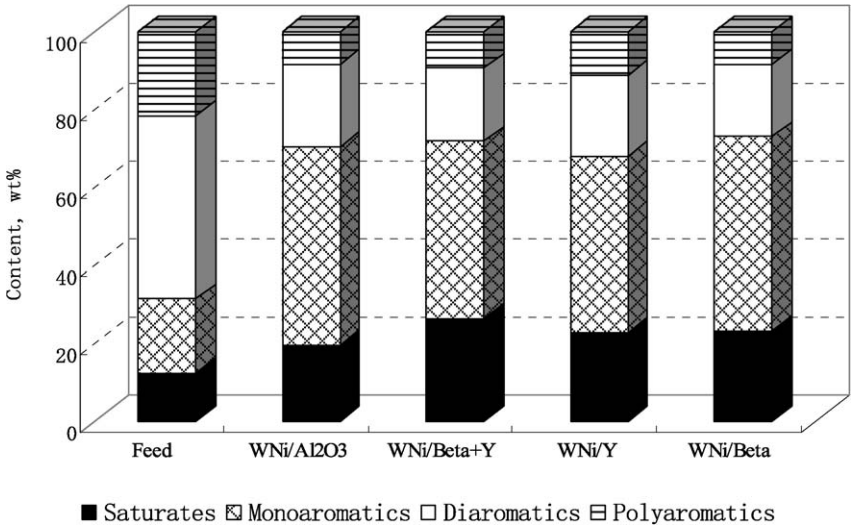

Fig. 9. The saturates and aromatics distribution in feed and hydrotreated products on WNi/Al_2O_3, WNi/Beta, WNi/Y, and WNi/Beta + Y.

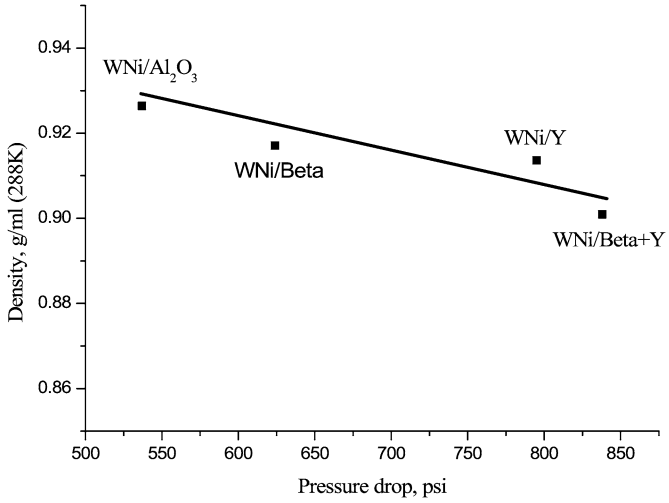

Fig. 10. The relationship between pressure drop and product density.

nitrogen and 98 wt% of sulfur could be removed from the LCO on the zeolite-containing catalysts under the present reaction conditions. HDN activity among the three zeolite-containing catalysts was identical. The HDS activity of WNi/Beta + Y and WNi/Beta was higher than that of WNi/Y.

The increase in cetane index for the all catalysts was in the range of 4.3–5.2. The addition of the modified zeolites did not result in a considerably improved cetane index compared with WNi/Al_2O_3. As shown in Fig. 9, after hydrogenation, about 50–60% of polyaromatics and 55–60% of diaromatics were converted into monoaromatics on all the catalysts. Owing to high acidity, 3.3–6.9% more saturate hydrocarbons were produced on the zeolite-containing catalysts than that on WNi/Al_2O_3. Polyaromatics hydrogenation proceeds via successive steps, each of which is a reversible reaction [41]. Based on thermodynamics, the hydrogenation reactivity of aromatics decreases in the following order: polyaromatics > biaromatics > monoaromatics [41]. The hydrogenation of the monoaromatics is difficult and attained only when the temperature is higher than approximately 673 K [42]. The saturation of aromatics increases in the following order: WNi/Beta + Y > WNi/Beta > WNi/Y > WNi/Al_2O_3. After hydrotreating, only 7.1–14.0 wt% of aromatics was converted into saturates, resulting in only a small increase in cetane index. To further increase cetane index, some of the saturated aromatics structures must be opened to form paraffins and isoparaffins.

The main purpose of diesel hydroupgrading is to remove the impurities and partial hydrogenation of aromatics. Therefore, diesel fraction conversion obtained on $MoNi(MoCo)/Al_2O_3$ or WNi/Al_2O_3 from hydrotreating diesel fractions in most refineries is very lower. In our case, the conversion on WNi/Al_2O_3 reaches to 8.55 wt%. Such a high conversion can be attributed to the more secondary cracking of the hydrogenated products in a batch autoclave reactor than in a flow reactor, due to a longer period of contact with the catalyst. Compared with WNi/Al_2O_3, the conversions of the zeolite-containing catalysts are much higher. Most refineries intend to obtain as high diesel yield as possible. Thus, the high conversion usually is not acceptable by refineries, though very low sulfur, nitrogen, and aromatics can be achieved. Among the three zeolite-containing catalysts, WNi/Beta has the lowest conversion (10.05 wt%) and is most likely improved to approach the conversion of WNi/Al_2O_3 via further proper modification of the zeolite beta.

The correlation of the <406 K conversion and the acidity showed that higher acidity led to higher conversion. The conversion followed the same order of the acidity: WNi/Beta + Y > WNi/Y > WNi/Beta > WNi/Al_2O_3. From the distillation curve, it can be seen that there are about 0.8–2.5 wt% (Table 6) of fractions with boiling ranges higher than the end boiling point of the feed, which means that some larger molecules are formed after the hydrotreating reaction. Heavy molecules may form due to pressure swings or thermal soaking, or via disproportionation reactions or fusion of aromatics. Generally, the disproportionation reaction or fusion of aromatics occurs readily on acidity sites. Thus the quantities of the fractions higher than the end boiling point of the feed for the four catalysts are in the same order as the acidity of the catalysts: WNi/Beta + Y ∼ WNi/Y > WNi/Beta > WNi/Al_2O_3. There-

fore, higher acidity not only increases the conversion, but also causes some fractions with boiling points higher than the boiling point of the feed. Decreasing the acid site density in zeolites can efficiently suppress the coke formation reaction [43].

During the activity evaluation in the autoclave reactor, a sharp pressure drop was observed at around 463 K, indicating that a large amount of hydrogen was consumed and the hydrogenation reaction began at around this temperature. The overall pressure change (drop) can be taken as an indication of the extent of overall reaction involved, which can be reflected by the density of products. Fig. 10 illustrates the relationship between the pressure drop and the product density. A good linear relationship shows that the extent of all reactions in the autoclave reactor can be predicted by the pressure drop.

The higher HDN, HDS, and HDA activities of the three zeolite-containing catalysts were associated primarily with the enhanced hydrogenation activity and increased acidity. The XPS results reveal no correlation between the sulfidation degree of W and Ni and reaction activities; therefore, the large difference in hydrogenation activity could not result from the variation in the extent of sulfidation. Although a dominant amount of W and Ni species was located in the interior surface of all catalysts after calcination and sulfidation, the pore sizes of these catalysts were sufficiently large so as to be accessible by the reactant molecules of LCO. Thus, the different distributions of sulfided W and Ni outside and inside the pores seemingly could not lead to the large difference between WNi/Al_2O_3 and zeolite-containing catalysts either. The enhanced hydrogenation activity was likely associated with the size of hydrogenation active sites, WS_2. The single-slab structure [called type-I Co(Ni)–Mo(W)–S] interacted strongly with the support, whereas the multiple-slab form [called type-II Co(Ni)–Mo(W)–S] had weak interaction with the support and exhibited greater hydrogenation activity [44,45]. Multilayered WS_2 slabs provided a higher density of multivacancies compared with single-layered or thin slabs. This could facilitate π-complexation of the aromatic ring on multilayered WS_2 slabs relative to single-layered or thin slabs. Consequently, the hydrogenation activity of the catalyst was greatly improved. Vradman et al. also concluded that the higher stacking number of WS_2 slabs favoured an increase in HYD activity [40]. After the addition of zeolites, the WS_2 crystallite sizes on the catalysts increased significantly, producing the substantially enhanced hydrogenation performance of the catalysts. The acidity was likely another important factor boosting the activities of zeolite-containing catalysts. The addition of zeolites led to a 0.140–0.206 mmol/g increase in acidity. The high acidity of the zeolite-containing catalysts not only enhances HDS via hydroisomerization, but also facilitates the ring opening of saturated aromatics, facilitating further hydrogenation of the aromatics. It is noted that although the sizes of the surface WS_2 slabs were similar for WNi/Beta and WNi/Y, and WNi/Y had higher acidity than WNi/Beta (0.506 vs. 0.408 mmol/g), WNi/Beta had greater HDS and HDA activities. Therefore, the acidic strength seemingly played a more important role than the total acidity in controlling HDS and HDA activities. Due to the greater number of strong acidic sites on WNi/Beta compared with WNi/Y (0.151 vs. 0.08 mmol/g), higher HDS and HDA activities were achieved by WNi/Beta. After the zeolite beta and/or zeolite Y were added to the catalysts, HDN and HDA activities increased much more significantly than HDS activity. Based on the mechanisms of HDN and HDA, the incorporation of zeolites is known to enhance the hydrogenation performance of the catalysts more pronouncedly than the increase in acidity.

To gain new and deep insight into W(Mo)–Ni(Co) hydrotreating catalysts, one must study the changes of reactivity, structures, and physicochemical properties of the catalysts with time. Through the evolution of the specific species and sites with time, more detailed information can be obtained about the catalysts and reactions involved.

4. Conclusions

The addition of modified zeolite beta and zeolite Y enhanced the overall acidity of the W–Ni catalysts. The acidity of the modified zeolite Y-containing catalyst was higher than that of the zeolite beta-containing catalyst. The incorporation of zeolite Y led mainly to an increase in weak acidity, whereas incorporation of zeolite beta caused an increase in strong acidity.

Very small tungsten and/or nickel sulfide clusters contained more than a stoichiometric amount of sulfur. W and Ni exhibited a very high degree of sulfidation in all catalysts. Nickel species in WNi/Al_2O_3 interacted with the support more strongly than they did in the zeolite-containing catalysts. Among the zeolite-containing catalysts, the sulfidation degree decreased in the order WNi/Y > WNi/Beta + Y > WNi/Beta. A considerable amount of W and Ni migrated into the bulk after calcination. The W and Ni further migrated into the support after sulfidation.

For all catalysts, WS_2 presented in a typical layered structure on the support. With increased zeolite content, the WS_2 slabs grew large, and the number of layers increased. The size of WS_2 was related mainly to the distribution of WS_2 on the surface of Al_2O_3, irrespective of the type of zeolite. Compared with WNi/Al_2O_3, the distribution of the slab length and the number of layers for the zeolite-containing catalysts were much broader.

Compared with WNi/Al_2O_3, the zeolite-containing catalysts exhibited much higher HDN, HDS, and HDA activities. HDN activity among the three zeolite-containing catalysts was similar. HDS activity of WNi/Beta + Y and WNi/Beta was higher than that of WNi/Y. The higher HDN, HDS, and HDA activities of the three zeolite-containing catalysts are associated mainly with enhanced hydrogenation activity and increased acidity. The addition of zeolites to the catalysts enhanced hydrogenation more significantly than it increased acidity.

After hydrogenation, most aromatics were converted to monoaromatics. The saturation of aromatics increased in the order WNi/Beta + Y > WNi/Beta > WNi/Y > WNi/Al_2O_3.

The higher acidity led to higher conversions. The conversions of the zeolite-containing catalysts were much higher than the conversion of WNi/Al_2O_3. Some molecules larger than those in the feed were formed after the hydrotreating reaction. The quantities of these large molecules were also in the same

order as the acidity of the catalysts. Adding the modified zeolites did not significantly improve the cetane index.

Acknowledgment

The authors are grateful to the Atlantic Innovation Funding for funding this project.

References

[1] C. Song, Catal. Today 86 (2003) 211–263.
[2] R. Shafi, G.J. Hutchings, Catal. Today 59 (2000) 423–442.
[3] V. Meille, E. Schulz, M. Lemaire, M. Vrinat, J. Catal. 170 (1997) 29–36.
[4] T. Kabe, A. Ishihara, Q. Zhang, Appl. Catal. A 97 (1993) L1–L9.
[5] F. Bataille, J.L. Lemberton, P. Michaud, G. Perot, M. Vrinat, M. Lemaire, E. Schulz, M. Breysse, S. Kasztelan, J. Catal. 191 (2000) 409–422.
[6] E. Lecrenay, K. Sakanishi, I. Mochida, Catal. Today 39 (1997) 13–20.
[7] T. Isoda, S. Nagao, Y. Korai, I. Mochida, Am. Chem. Soc., Prepr. Div. Petrol. Chem. 41 (1996) 559–565.
[8] I. Isoda, S. Nagao, X. Ma, Y. Korai, I. Mochida, Energy Fuels 10 (1996) 1078–1082.
[9] F. Bataille, J.L. Lemberton, G. Pérot, P. Leyrit, T. Cseri, N. Marchal, S. Kasztelan, Appl. Catal. A: Gen. 220 (2001) 191–205.
[10] T. Isoda, S. Nagao, Y. Korai, I. Mochida, Sekiyu Gakkaishi 41 (1) (1998) 22–30.
[11] D. Li, A. Nishishjima, D.E. Morris, G.D. Guthrie, J. Catal. 188 (1999) 111–124.
[12] S. Bendezu, R. Cid, J.L.G. Firro, A. Lopez Agudo, Appl. Catal. A 197 (2000) 47–60.
[13] N. Kunisada, K. Choi, Y. Korai, I. Mochida, K. Nakano, Appl. Catal. A 276 (2004) 51–59.
[14] D. Solis, T. Klimova, R. Cuevas, J. Ramirez, A. Lopez-Agudo, Catal. Today 98 (2004) 201–206.
[15] C. Marin, J. Escobar, E. Galvan, F. Murrieta, R. Zarate, H. Vaca, Fuel Process. Technol. 86 (2004) 391–405.
[16] A. Hassan, S. Ahmed, M.A. Ali, H. Hamid, T. Inui, Appl. Catal. A 220 (2001) 59–68.
[17] J. Scherzer, Catalytic Materials: Relationship between Structure and Reactivity, ACS Monograph, No. 248, Washington, DC, 1984, pp. 157–159.
[18] Yu. Lsaev, J.J. Fripiat, J. Catal. 182 (1999) 257–263.
[19] G. Garralon, V. Fornes, A. Corma, Zeolites 8 (1988) 268–272.
[20] A. Corma, V. Fornes, J.B. Monton, A.V. Orchilles, J. Catal. 107 (1987) 288–295.
[21] J.P. Angevien, M.K. Mitchell, M.S. Oleck, S.S. Shih, US Patent 4612108 (1985), to Mobil Oil Corporation.
[22] M.A. Ali, T. Tasumi, T. Masuda, Appl. Catal. A 233 (2002) 77–90.
[23] D.W. Breck, H. Blass, G.W. Skeels, US Patent 4503023 (1985), to Union Carbide Corporation.
[24] S. Bendezú, R. Cid, J.L.G. Fierro, A. López Agudo, Appl. Catal. A 197 (2000) 47–60.
[25] K.T. Ng, D.M. Hercules, J. Phys. Chem. 80 (1976) 2094–2102.
[26] L. Salvati Jr., L.E. Makovsky, J.M. Stencel, F.R. Brown, D.M. Hercules, J. Phys. Chem. 85 (1981) 3700–3707.
[27] R. Cid, J.L.G. Fierro, A. López Agudo, Zeolites 10 (1990) 95–100.
[28] B. Pawelec, L. Daza, J.L.G. Fierro, J.A. Anderson, Appl. Catal. A: Gen. 145 (1996) 307–322.
[29] B. Pawelec, J.L.G. Fierro, J.F. Cambra, P.L. Arias, J.A. Legarreta, G. Vorbeck, J.W. de Haan, V.H.I. de Beer, R.A. van Santen, Zeolites 218 (1997) 250–259.
[30] R.B. Shalvoy, P.J. Reucroft, J. Vac. Sci. Technol. 16 (1979) 567–573.
[31] L. Portela, P. Grange, B. Delmon, J. Catal. 156 (1995) 243–254.
[32] S. Damyanava, L. Petrov, P. Grange, Appl. Catal. A 239 (2003) 241–252.
[33] W.J.J. Welters, G. Vorbeck, H.W. Zandbergen, J.W. de Haan, V.J. de Beer, R.A. van Santen, J. Catal. 150 (1994) 155–169.
[34] J. Scherzer, A.J. Gruia, Hydrocracking Science and Technology, Marcel Dekker, New York, 1996, pp. 70–75.
[35] R. Cid, P. Atanasova, R. Lopez Cordero, J.M. Palacios, A. Lopez Agudo, J. Catal. 182 (1999) 328–338.
[36] H.R. Reinhoudt, E. Crezee, A.D. van Langeveld, P.J. Kooyman, J.A.R. van Veen, J.A. Moulijn, J. Catal. 196 (2000) 315–329.
[37] Y.W. Li, X.Y. Pang, B. Delmon, J. Mol. Catal. A: Chem. 169 (2001) 259–268.
[38] B. Scheffer, N.J.J. Dekker, P.J. Mangnus, J.A. Moulijn, J. Catal. 121 (1990) 31–46.
[39] J. Leglise, J.M. Manoli, C. Potvin, G. Djega-Mariadassou, D. Cornet, J. Catal. 152 (1995) 275–290.
[40] L. Vradman, M.V. Landau, M. Herskowitz, Fuel 82 (2003) 633–639.
[41] B.H. Cooper, B.B.L. Donnis, Appl. Catal. A 137 (1996) 203–223.
[42] M. Bouchy, P. Dufresne, S. Kasztelan, Ind. Eng. Chem. Res. 31 (1992) 2661–2669.
[43] J. Scherzer, A.J. Gruia, Hydrocracking Science and Technology, Marcel Dekker, New York, 1996, pp. 117–120.
[44] H. Topsoe, B.S. Clausen, N.-Y. Topsoe, P. Zeathen, Stud. Surf. Sci. Catal. 53 (1989) 77–85.
[45] H. Topsoe, B.S. Clausen, Appl. Catal. 25 (1986) 273–293.